

# The Carlina-type diluted telescope: Stellar fringes on Deneb

H. Le Coroller<sup>1,2</sup>, J. Dejonghe<sup>3,\*</sup>, F. Hespeels<sup>4,1</sup>, L. Arnold<sup>1</sup>, T. Andersen<sup>5</sup>, P. Deram<sup>1</sup>, D. Ricci<sup>6,1</sup>, P. Berio<sup>3</sup>, A. Blazit<sup>3</sup>, J-M. Clausse<sup>3</sup>, C. Guillaume<sup>1</sup>, J.P. Meunier<sup>1</sup>, X. Regal<sup>1</sup>, and R. Sottile<sup>1</sup>

<sup>1</sup> Aix Marseille Université, CNRS, OHP (Observatoire de Haute Provence), Institut Pythéas UMS 3470, 04870 Saint-Michel-l'Observatoire, France

<sup>2</sup> Laboratoire d'Astrophysique de Marseille, Pôle de l'Étoile Site de Château-Gombert, 38, rue Frédéric Joliot-Curie, 13388 Marseille cedex 13, FRANCE

e-mail: herve.lecoroller@lam.fr

<sup>3</sup> Université Nice-Sophia Antipolis, Observatoire de la Côte d'Azur, CNRS UMR 6525, BP 4229, F-06304 Nice Cedex, France

<sup>4</sup> University of Namur (UNamur), research Center for Physics of Radiation and Matter (PMR-LARN), 61 rue de Bruxelles, B-5000 NAMUR

<sup>5</sup> Lund Observatory, Box 43, SE-221 00 Lund, Sweden

<sup>6</sup> Instituto de Astronomía – UNAM, Km 103 Carretera Tijuana Ensenada, 422860 Ensenada, B. C., Mexico.

accepted October 04, 2014

## ABSTRACT

**Context.** The performance of interferometers has largely been increased over the last ten years. But the number of observable objects is still limited due to the low sensitivity and imaging capability of the current facilities. Studies have been done to propose a new generation of interferometers.

**Aims.** The Carlina concept studied at the Haute-Provence Observatory consists in an optical interferometer configured as a diluted version of the Arecibo radio telescope: above the diluted primary mirror made of fixed co-spherical segments, a helium balloon or cables suspended between two mountains and/or pylons, carries a gondola containing the focal optics. This concept does not require delay lines.

**Methods.** Since 2003, we have been building a technical demonstrator of this diluted telescope. The main goals of this project were to find the opto-mechanical solutions to stabilize the optics attached under cables at several tens of meters above the ground, and to characterize this diluted telescope under real conditions. In 2012, we have obtained metrology fringes, and co-spherized the primary mirrors within one micron accuracy. In 2013, we have tested the whole optical train: servo loop, metrology, and the focal gondola.

**Results.** We obtained stellar fringes on Deneb in September 2013. In this paper, we present the characteristics of these observations: quality of the guiding,  $S/N$  reached, and possible improvements for a future system.

**Conclusions.** By detecting fringes on Deneb, we confirm that the entire system conceptually has worked correctly. It also proves that when the primary mirrors are aligned using the metrology system, we can directly record fringes in the focal gondola, even in blind operation. It is an important step that demonstrates the feasibility of building a diluted telescope using cables strained between cliffs or pylons. Carlina, like the MMT or LBT, could be one of the first members of a new class of telescopes named Large Diluted Telescopes. Its optical architecture has many advantages for future projects: Planet Formation Imager, Post-ELTs, Interferometer in space.

**Key words.** Instrumentation: interferometric, interferometers – Instrumentation: high angular resolution – Telescopes – Instrumentation: adaptive optics – Protoplanetary disks – Planetary systems

## 1. Introduction

The last ten years have seen a significant increase in scientific publications making use of images based on optical long-baseline interferometry. The sensitivity and imaging capability of the interferometers have progressed. We are able to recombine up to 6 telescopes such as with the MIRC instrument on CHARA (Ten Brummelaar et al. 2010). Nevertheless, the number of observable objects with this technique stays limited due to the low sensitivity and the modest number of telescopes we are able to recombine simultaneously (max. 6). The current limitations of the interferometers lie also in their ability to detect highly contrasted features (Mennesson 2014).

Studies are under way to propose a new generation of interferometers, more sensitive with higher imaging capabilities than current systems. More than 6 telescopes are required to reconstruct images of complex objects (Berger et al. 2012). They should be able to produce images at very high contrast using coronagraphic techniques (e.g. Lacour et al. 2014). To reach this goal, the interferometers have to be improved along their full optical path. The number of reflections between the primary mirrors and the focal instrument has to be minimized to limit the flux lost in numerous reflexions. In this spirit, the OHANA team has studied the possibility to transport the light in optical fibers (Perrin et al. 2000; Woillez et al. 2005). The focal instrument can be optimized for example with integrated optics with better throughput and with photometric calibration

\* First and Second authors contributed equally

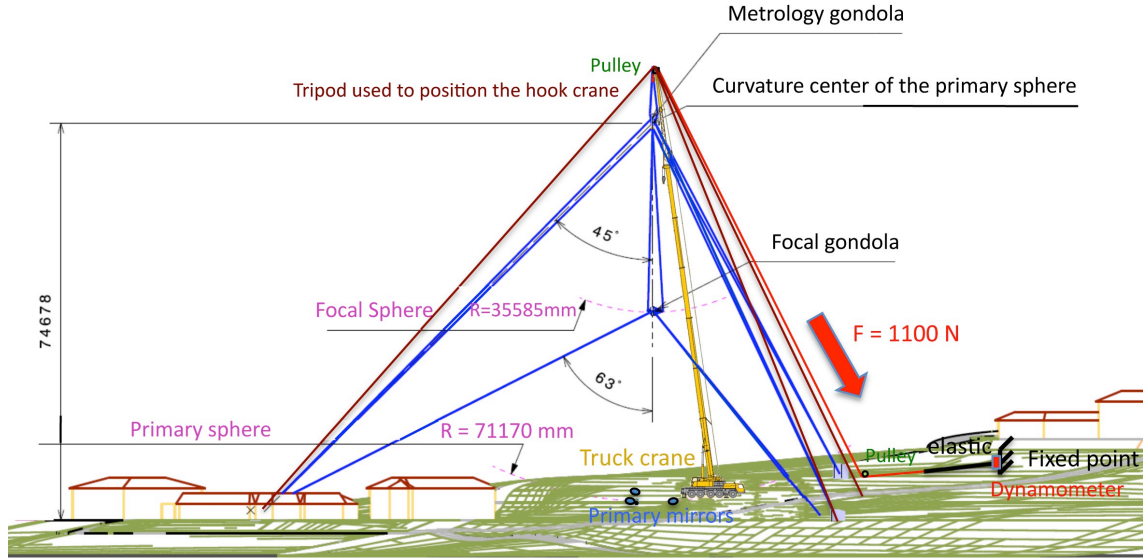


**Fig. 1.** The Carlina-OHP experiment: In September 2013, the helium balloon (Paper I & Paper II) was replaced by a truck crane. The thickness of the cables, and the diameter of the primary mirrors (25cm) have been exaggerated to be seen on this scale drawing. An elastic rope attached to the ground passes through a pulley at the top of the crane and pulls on the same cable, with the same force (1100 N) as the helium balloon.

capability (Berger et al. 1999). It is crucial to damp vibrations of sensitive parts, such as mirror mounts, delay lines, etc.

At the Haute-Provence observatory, we have studied a new concept for a diluted telescope. As described in two previous papers (Le Coroller et al. 2004, Paper I; Le Coroller et al. 2012b, Paper II), it is configured as a diluted version of the Arecibo radio telescope: above the diluted primary mirror made of fixed co-spherical segments, a helium balloon (or a crane) carries a gondola containing the focal optics. It works without delay lines and the focal gondola is the only moving part. With this simple optical train, in the future, tens or hundreds of mirrors could be added in the pupil to improve the imaging capability and sensitivity of the interferometer.

The biggest difficulty for this system is to stabilize the focal gondola that moves to track the stars, attached to cables at tens of meters above the ground. Indeed, the fringes move on the focal sphere with the Earth rotation and the focal optic has to track them exactly at the correct velocity to avoid that they drift on the camera during the exposure time. The speed and the maximum velocity drift of the focal gondola beyond which the fringes are totally blurred are of the same order of magnitude as the ones of a delay line of an interferometer having a baseline of equivalent length. This is a challenge for a cable-suspended focal gondola (see Table 1 of Dejonghe et al. 2014). The main goals of this project were thus to find opto-mechanical solutions to stabilize the optics attached under cables, and to test this interferometer in real conditions, i.e. to obtain fringes that stay in the field of view of the focal optic, and that move slowly enough to be frozen in a short exposure ( $\approx 5$  ms). Note that the first fringes have been obtained in May 2004 with two closely-spaced primary segments providing 40 cm baseline, and a CCD on the focal gondola (Paper I). These first encouraging results had proved that we can track the stars with a gondola attached by cables 35 m above the ground. But, the two primary mirrors were easily co-spherized because they were adjacent. Moreover, the maximum velocity drift acceptable to freeze the fringes in a short exposure is proportional to the fringes size ( $\lambda \frac{f}{B}$ ), i.e. to the aperture ratio  $\frac{f}{B} = 35/0.4 = 88$  in 2004. A future scientific project would have much bigger baselines, and would work

at a larger aperture ratio (typically  $F/D = 2 - 3$ ) to minimize the altitude of the focal gondola. In this case, the maximum velocity drift to freeze the fringes is 44 times smaller than in our experiment of 2004. In order to test the Carlina architecture in more realistic conditions than in 2004, we decided to validate the concept at  $F/3.5$  (baselines of 5–10 m).

In 2011–2012, we obtained metrology fringes, and we co-spherized distant primary mirrors (baselines 5–10 m) within one micron accuracy (Paper II). The opto-mechanical design, the metrology system and the servo loops have been largely described in Paper I, Paper II, and in several conference proceedings (Le Coroller et al. 2012a; Dejonghe et al. 2014).

In this paper, we focus on the observation performed in September 2013. In Sect. 2, we recall quickly the main prototype characteristics that are relevant for the data reduction (baseline, photon counting camera, guiding camera characteristics, etc.). In Sect. 3, we present the data recorded in September 2013. Data reduction, and fringes on Deneb are shown at Sect. 4. The guiding behaviour is described in Sect. 5. A discussion is provided in Sect. 6 and the conclusion is given in Sect. 7.

## 2. Carlina prototype characteristics

Carlina can be divided into four blocks: The primary mirrors, the focal gondola, the metrology gondola and the holding system (Fig. 1 of Paper II). Carlina specifications are provided in Table A.1 of Paper II, and in Table 1 of Dejonghe et al. (2014). Here, we just recall the main characteristics of the prototype built at the Haute-Provence observatory:

The primary mirror is made of three segments positioned on a 71.2 meter radius sphere (Fig. 1), forming three baselines of respectively 5, 9 and 10.5 meters (Paper II). The metrology gondola (Paper II), and the focal gondola are then respectively at 71.2 m and 35.6 m above the ground. From 2003 to 2012, the metrology and focal gondolas were carried by cables attached under a helium balloon. But experience proved that the use of a helium balloon exhibits a serious drawback: it requires a complete disassembly of the installation every morning, and a re-assembly every evening! The entire instrumental setup using

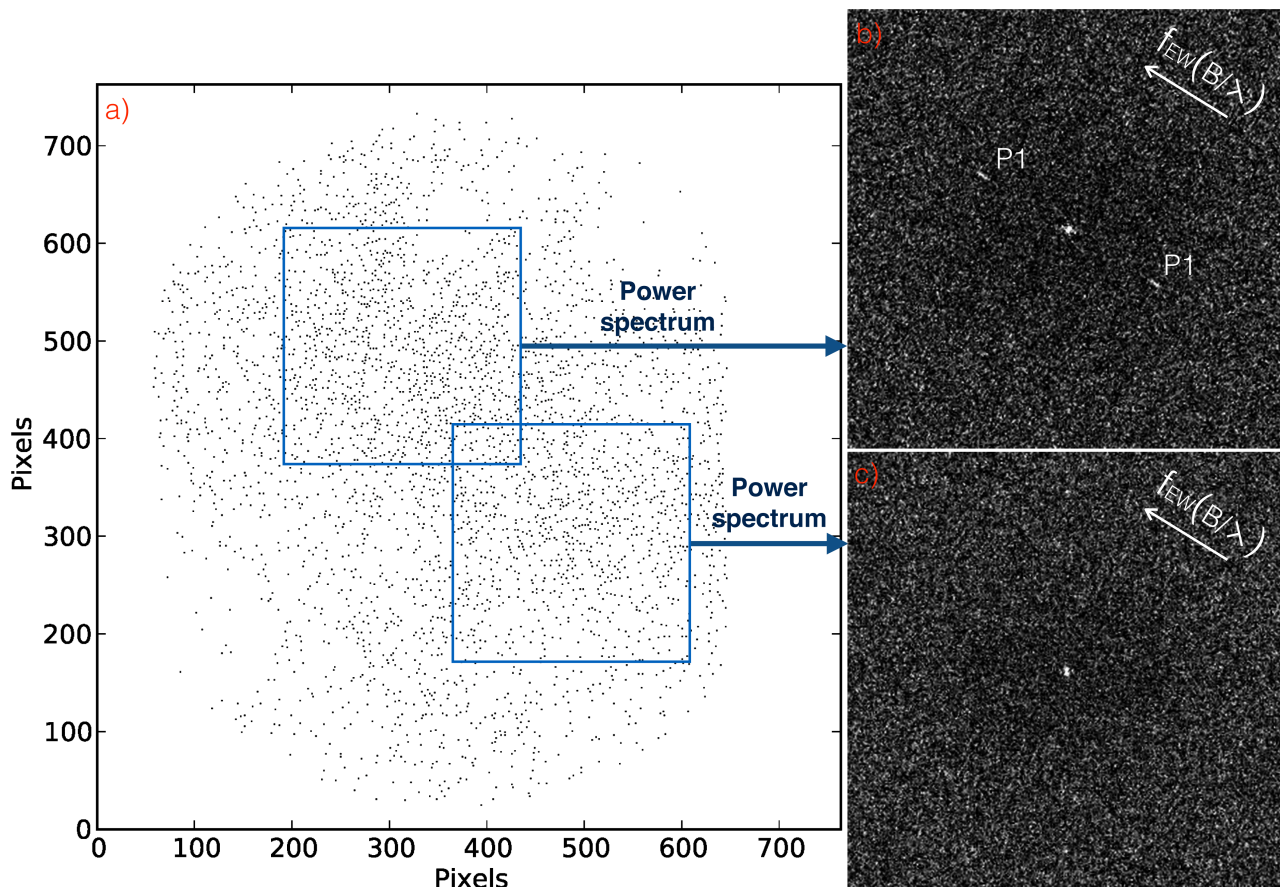


**Fig. 2.** a) Binary image (cropped to  $761 \times 761$  pixels) obtained on Deneb in 1 ms exposure time with the Carlina photon counting camera. The light that falls on the CCD comes from the intensifiers of circular shape. This image contains 3524 Photons. b) Square modulus of the Fourier Transform of the top left image (blue square of  $245 \times 245$  pixels). In this part of the image, we detect the fringe peaks of the 5 m baseline (P1 mark). The intensities in the power spectrum are represented using a linear scale. The white arrow indicates the direction and the norm of the spatial frequency of the 5m baseline (oriented East-West) at 510 nm. Only two images among the Deneb data allow a direct detection of the fringes (in an individual frame without adding several power spectra). c) No fringes are detected in the power spectrum of the bottom right image. i.e. the fringes are located in the top left part of the image a).

the balloon was not designed to resist to winds above 20 km/h. The balloon has thus been replaced by a lifting crane (Fig. 1) for the last observation run, in September 2013 (Dejonghe et al. 2014). This holding system behaves as the pylons that could be used for a future project (Paper II).

In 2013, we have also simplified the focal gondola (Dejonghe et al. 2014) by removing the pupil densifier (Labeyrie 1996). The required guidance accuracy (0.1 arcsec) was indeed impossible to reach without an embedded fine guiding system. The Fizeau focal recombiner used to record the data presented in this paper is only equipped with a corrector of spherical aberration, and guiding and science cameras. A dichroic mirror reflects the red part of the light onto the guiding camera ( $\lambda > 700$  nm) and lets the blue light ( $\lambda < 700$  nm) pass toward a photon-counting science camera (Blazit et al. 2008). The diameter of the field of view of the science camera is 2 arcsec. The field of view of the guiding camera (AVT Guppy F-038 NIR from Allied Vision Technologies company) is 40 arcsec. The science camera uses two intensifiers (Blazit et al. 2008). The intensifiers feed a  $1024 \times 1024$  pixels CCD<sup>1</sup>. The guiding and science images are sent to a ground-based PC by optical fibers with a maximum transfer rate of 33 science images per second. The science

images are cropped to  $761 \times 761$  pixels corresponding approximately to the size of the circular intensifiers (Fig. 2).

### 3. Observing log

We have observed three stars during a run of 4 nights from September 2 to 5, 2013:  $\gamma$  And, Deneb ( $\alpha$  Cyg), and  $\delta$  And. Fringes were obtained on Deneb during the night of the run with the best atmospheric conditions (Table A.1). A green filter centred at  $\lambda = 510$  nm with 84 nm bandwidth has been used at the entrance of the science camera. The exposure time of the science camera was adjusted between 1 ms and 10 ms. With only three mirrors (Paper II, and Dejonghe et al. 2014) our prototype can observe only near Zenith (declination:  $40^\circ < \delta < 50^\circ$ ). Moreover, the duration of observation depends on the declination of the star. Fig. 3 shows the observing windows for Deneb. We also recorded images with the guiding camera to evaluate the stability of the focal gondola during tracking.

<sup>1</sup> MV-D1024-CL CMOS model from the Photon Focus company



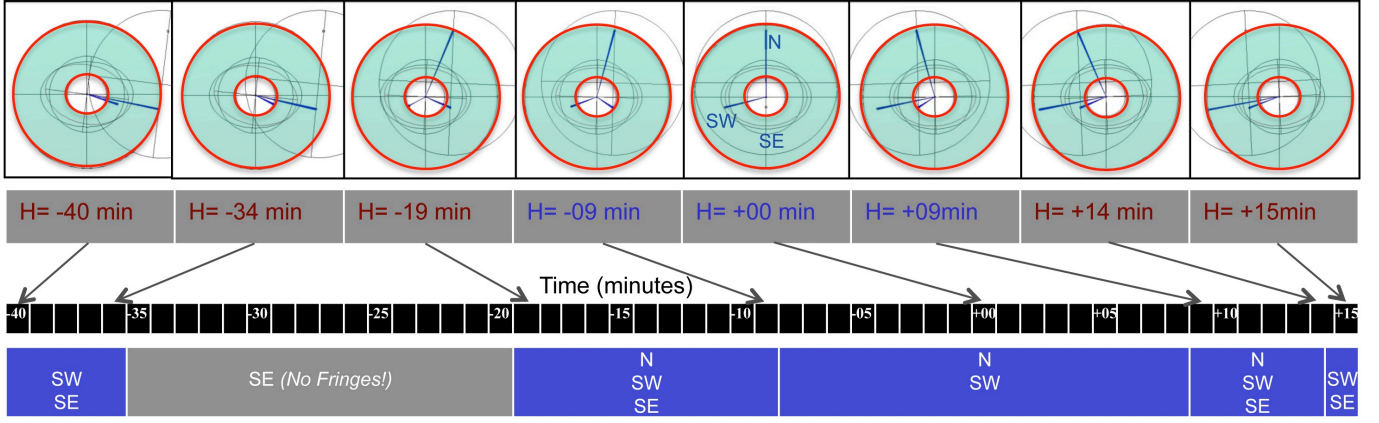


**Fig. 3.** Top: Zemax ray-tracing software views from above the focal gondola on the optical axis. These graphs show the optical rays (blue lines) for the declination of the star Deneb at several hour angles ( $-40 \text{ min} < H < +15 \text{ min}$ ). In this projected view, each mirror (N, SW, SE) is at the end of a blue line. It falls in the Mertz field of view if it is located between the two red circles (in the blue area). The central obscuration is due to the central hole of the Mertz corrector (see Fig. 2 & Fig. 4 of Paper I): when a primary segment is aligned with this hole (i.e. the focal gondola is aligned with this segment and the star), the light is lost (the lost light can be blocked by a mask in the pupil plane, to avoid directly illuminating the camera). A graph is shown each time a primary mirror enters in or exits from the Mertz field of view. Note that the North mirror is represented, but during the observation of Deneb it was not aligned, and was masked. Thus, we expected fringes on Deneb only when the SW and SE mirrors are in the field of view. Bottom: We give the name of the primary mirrors (N, SW, SE) that are in the field of view of the Mertz corrector during the tracking of Deneb. From 35 min to 20 min before the transit only the SE mirror is in the field of view of the Mertz corrector, and no fringe acquisition is possible. We have recorded data on Deneb during 1 min 30 s starting 10 min before the transit (transit at  $H = 00 \text{ min}$  i.e. 21:18:28 UT on September 05, 2013), and during 5 min, 9 min 30 s after the transit (see the observing log of Table A.1). During 18 min around the transit, the SE mirror of the small baseline is not in the field of view of the Mertz corrector (confirmed during the observation: Table A.1).

#### 4. Data reduction

The binary images (Fig. 2) of the science camera were transformed into FITS format using a C++ script calling routines from the *quarklib* library<sup>2</sup>.

During 1 h around the transit, the motion of the fringe peak can be approximated by a counterclockwise linear rotation of  $\approx 0.68^\circ$  per degree of hour angle ( $\approx 0.17^\circ$  per min). Moreover, the width of the peak is proportional to the diameter of the primary mirrors (Rodier & Lena 1984, Rabbia 1989). It has been estimated in the image by using the power spectrum simulated in the laboratory (Fig. 4) giving  $\approx 3^\circ$  view from the center of the power spectrum i.e. it turns 1/10 eme of its width in about 2 min. So, we compute the power spectrum of a series of images by taking the sum of the squared modulus of the Fourier transform of 1000 frames ( $\approx 30$  seconds of acquisition) without rotation correction. Over a larger period, we align the fringe peaks (each one computed with 1000 images without rotation correction) by applying a rotation (without interpolation). Finally, we co-add all the computed power spectra.

A fringe peak is only detected on Deneb (Fig. 2 & Fig. 4) on September 5 between 21:08:30 UT and 21:33:00 UT on the 5 m baseline (that night, we worked only with two mirrors; the North aperture was closed). The fringe peak has a  $S/N = 5.4$  (Table 1) and it is at the expected shape and position. It is slightly elongated due to the relatively large bandwidth filter ( $\Delta\lambda = 84 \text{ nm}$ ) that we used (see Fig. 4).

##### 4.1. Signal to noise ratio

We estimate the signal to noise ratio of the fringe peak as:

$$\frac{S}{N} = \frac{I_{\text{Peak}} - \langle I_{\text{Bg}} \rangle}{\sigma_{\text{Bg}}} \quad (1)$$

<sup>2</sup> The library is currently being reimplemented as a C++ module for node.js, see <https://github.com/Nunkiini/node-fits>

where:

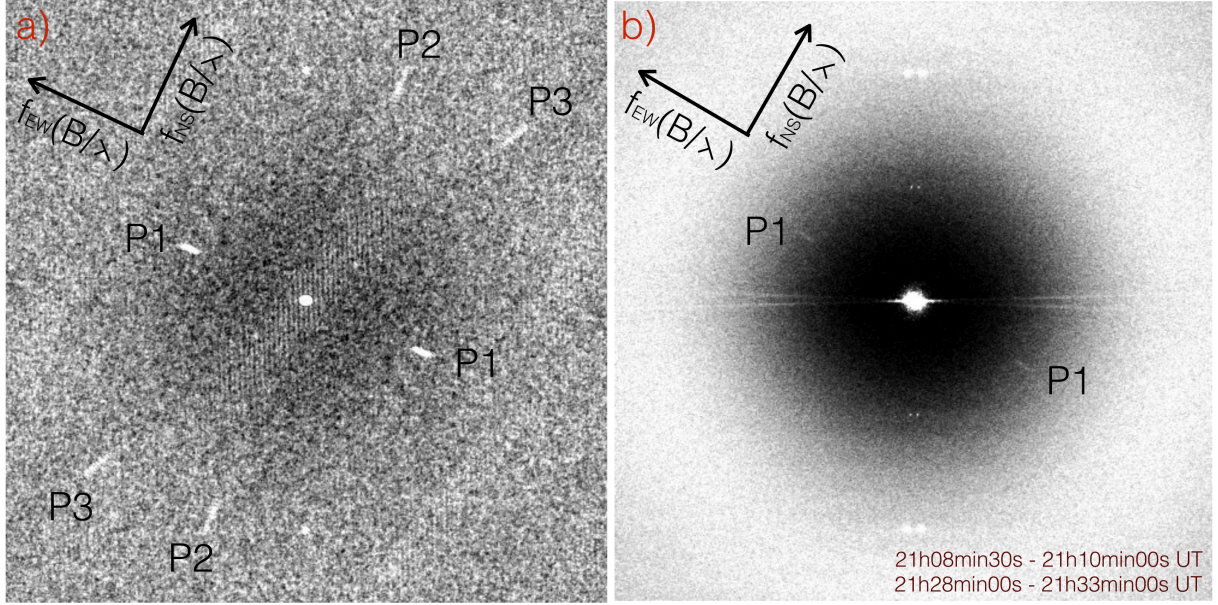
- $I_{\text{Peak}}$  is the intensity integrated in the fringe peak;
- $\langle I_{\text{Bg}} \rangle$  is the average intensity of the background around the fringe peak.
- $\sigma_{\text{Bg}}$  is the standard deviation of the background around the fringe peak.

Table 1 gives the  $S/N$  computed for the fringe peaks presented in Fig. 4 b). The highest signal to noise ratio ( $S/N = 6.6$ ) of the fringe peak is obtained if we remove the data from 21:30:00 to 21:33:00, showing that there is no signal during this period.

##### 4.2. Visibility

We have extracted a visibility from the power spectrum of Deneb using data recorded between 21:08:30 and 21:30:00 UT:  $V_{\text{Deneb}}(5 \text{ m}) = 0.03$ . The visibility measured on the single image shown at Fig. 2 gives  $V_{\text{Deneb}}(5 \text{ m}) = 0.3$ . These values are much smaller than the expected value of  $V_{\text{UD}}(5 \text{ m}) = 0.99$ . But, the visibility measurements are strongly degraded by atmospheric turbulence, and should be calibrated on a reference star. This is particularly relevant with our simple recombiner that works without spatial filtering, tip-tilt and photometric correction. The saturation of Deneb (Fig. 6) may also significantly decrease the visibility by removing more photons from the bright than the dark fringes (Blazit et al. 2008). Nevertheless, the goal here is simply to show that we are able to integrate the flux in the fringe peak using the Berio et al. (1998) method (to remove the so-called photon-centroiding hole) to measure a visibility point (Fig. 5). However, much more data (than 7000 images of 1 ms exposure time i.e. 7 s of integrated signal) would be required to compute a mean visibility with a good signal to noise ratio.





**Fig. 4.** a) Power spectrum of the Fizeau laboratory fringes obtained using a supercontinuum laser source in the focal plane of the Mertz corrector and a mask positioned on a lens just after (see L1 Lens in Fig. 3 of Le Coroller et al. 2012a and Fig. 12 of Dejonghe et al. 2014). The diameters of the three holes and their positions in the mask are adjusted using the Zemax ray tracing code to simulate the three stellar beams coming from the primary mirrors. The mask has been oriented to simulate the stellar fringes at the transit. P1, P2 and P3 indicate the position of the fringe peaks, respectively for the 5 m, 9 m and 10.5 m baselines. The vertically aligned dots are an artefact of the science camera (visible even if the camera is illuminated uniformly without fringes). b) Sum of all the power spectra computed for Deneb (3 000 images recorded before the transit and 10 000 images recorded after the transit: see log of the observations in Table A.1). The Earth rotation correction has turned the "artefacts" of the images taken before the transit counterclockwise, while they turned clockwise for the images taken after the transit. The intensities are represented using a linear scale. We see the Deneb fringe peaks of the 5 m baseline (P1). They are at the expected position with the same shape as in the laboratory (image a) using the green filter ( $\lambda = 510$  nm,  $\Delta\lambda = 84$  nm). The black arrows define the coordinate system of the panel. The  $f_{EW}$  arrow indicates the direction and the norm of the spatial frequency of the 5m baseline (oriented East-West) at 510 nm while the  $f_{NS}$  arrow shows the direction of the spatial frequency of the 10m baseline (oriented North-South). It has the same size as the  $f_{EW}$  arrow.

**Table 1.** Signal to noise ratio of the fringe peak for Deneb

Observing periods (hh:mm:ss)	Number of images	$S/N$ (with rotation correction)
21:08:30–21:10:00	3000	4.7
21:28:00–21:33:00	10 000	4.13
21:08:30–21:10:00 + 21:28:00–21:33:00	13 000	5.4
21:08:30–21:10:00 + 21:28:00–21:30:00	7000	6.6

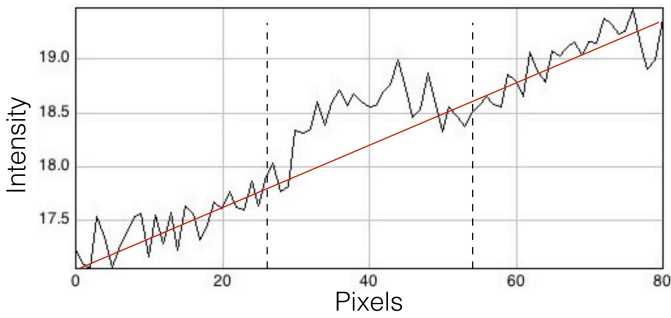


**Fig. 5.** Section view along the fringe peak of Deneb (P1 in the  $f_{EW}$  direction of Fig. 4) using data  $S/N=6.6$  (Table 1). To show the energy over the entire peak, a binning on its width (3 pixels in the FFT sampling) has been done before plotting. To extract a visibility, the energy of the peak is integrated between the two vertical dashed lines and above a polynomial fit.

## 5. Guiding characterisation

### 5.1. Analysis based on the science camera images

We have recorded data for Deneb continuously from 21:08:30 to 21:10:00 and from 21:28:00 to 21:33:00 but we do not detect fringes from 21:30:00 to 21:33:00 (6000 images). To analyse why the fringe peak is not present during all of the observations, we use the following property: the field of view of the science camera ( $\approx 2''$ ) has the same size as the typical seeing at OHP. The flux thus decreases immediately when the image becomes off-axis.

Fig. 6 shows in red the histogram of the data where we detect the fringes (21:08:30–21:10:00 UT + 21:28:00–21:30:00 UT; 7000 images), while the blue histogram is computed with the data without fringes signal (21:30:00–21:33:00 UT). Clearly, the red histogram shows more images at high flux than the blue one. 45% of the images of the data with fringes detected have more than 1800 photons while only 25% of the data without fringes exceed this value. Note that the histograms obtained on  $\gamma$  And

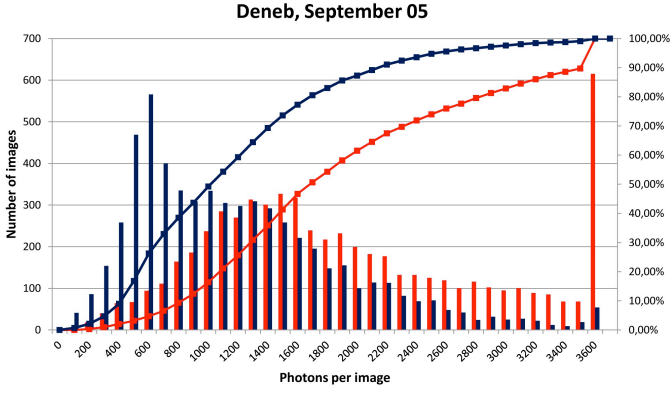


**Fig. 6.** Histograms of the photons per image. The line curves show the cumulative percentage of images of the histogram of the same color. No fringes were detected for the data of the blue histogram (data between 21:30:00 - 21:33:00 UT of Deneb). The red histogram correspond to the data where the fringes have been detected (21:08:30-21:10:00 UT + 21:28:00 - 21:30:00 UT). The large number of images at 3600 photons in the red histogram shows that Deneb slightly saturates the science camera. For the data of Deneb with fringes (in red), 45% of the images have more than 1800 photons (1800 is a little below half of the maximum flux on Deneb that is over the saturation level), while only 25% of the data without fringes (blue) exceed this value.

and *o And* have approximately the same shapes as the blue histogram on Deneb: 85–95% of the recorded images have less than 50% of their maximum flux, i.e. most of the time the fringes were not detected because the light was out of the science camera due to bad guiding. But it is not the only reason. In the next section, we show that the fringes are also blurred by guiding oscillations.

## 5.2. Analysis based on the guiding camera images

Guiding has been evaluated with only one aperture feeding the recombiner (Table A.1).

The top plot of Fig. 7 shows, during small and high amplitude guiding oscillations periods, the position of the focal image projected on an axis perpendicular to the fringes of the 5 m baseline, i.e. along the guiding CCD width, considering the optical design of the focal optics. Fig. 7 shows that the projected motion (perpendicular to the fringes) for a guiding period with large amplitude oscillations can be well approximated by straight lines with abrupt (practically instantaneous) changes in direction. Also, the velocity mean is linked to this global motion, and it is weakly affected by the atmospheric tip-tilt.

The mean velocity when guiding with large amplitude oscillations (blue curve in Fig. 7) is 0.2 fringe/ms (1 fringe with an exposure time of 5 ms). Fringes obtained with longer exposure times ( $\geq 5$  ms) are totally blurred. Note that during our observations, most of the time we were guiding with large amplitude oscillations ( $\approx 12''$ ) and we adjusted the exposure time to 5-10 ms (Table A.1), explaining why we did not detect fringes on  *$\gamma$  And* and *o And*. Moreover, each night  *$\gamma$  And* and *o And* have been observed with average wind speeds of 0.25–2.6 m/s (Table A.1). Deneb is the only star that has been observed during a long period (20h30 - 21h45 UT) without any wind and using very short exposure time (1 ms). The best seeing condition (0.9'') of the observing run was also obtained during that observation of Deneb.

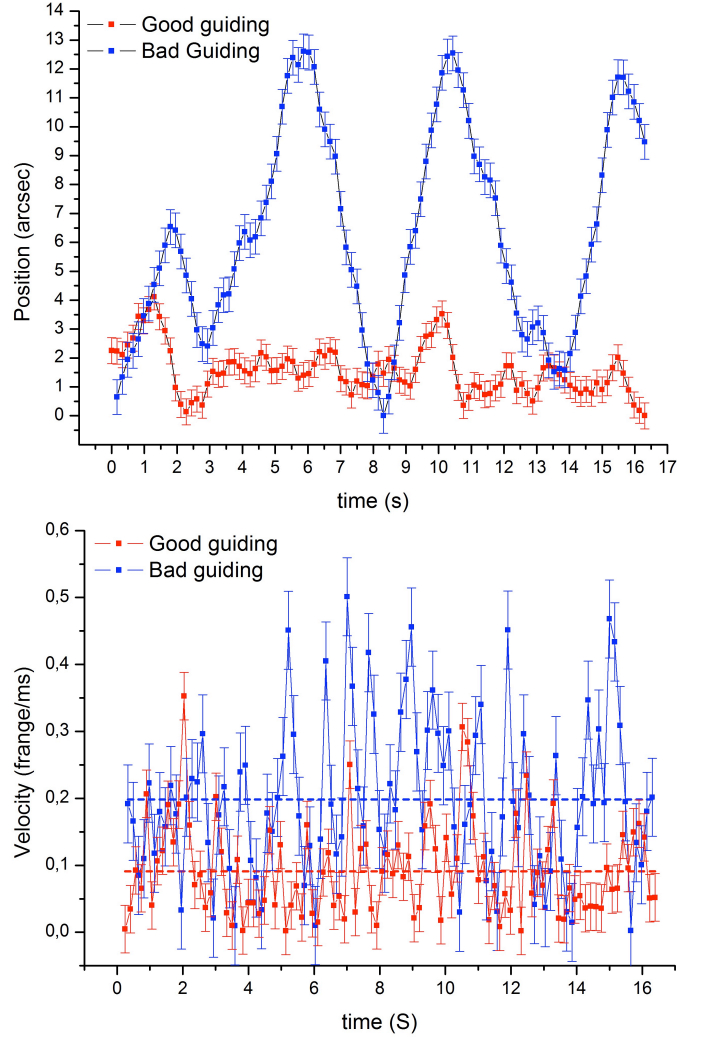


**Fig. 7.** Position (top), and its derivative (velocity at bottom) of the guiding focal image projected on an axis perpendicular to the fringes of the small baseline. The red and blue curves correspond to periods with small and large amplitude oscillations obtained on respectively *o And* (data selected among the recorded images between 22h57 and 23h00) and  *$\gamma$  And* (data selected in the first minute of the recorded images between 02h52 and 02h57). The unit of the vertical position axis is one arcsecond (1 pixel = 0.133'' on the guiding camera). The error bars of the top graph are the median "seeing" at the moment of the observation. The error bars of the bottom graph are the standard deviation ( $\sigma$ ) of the velocity points. The mean velocities are of 0.2 and 0.1 fringe/ms for guiding with large and small oscillations, respectively. One pixel of the guiding camera equals 6 fringes for the 5 m baseline. It is expressed in fringe/ms but for guiding with small amplitude oscillations, the fringes move probably less than 0.1 fringe/ms because this value is affected by the atmospheric tip-tilt.

## 6. Discussion

We have shown above that the low  $S/N$  of the detected fringe peak can largely be explained by guiding errors. Our prototype indeed works without tip-tilt correction, and we track the stars by winch control on 100 m long cables. Nevertheless, the measured guiding oscillations ( $\approx 12$  arcsec at 0.2 Hz) can be easily corrected by adding tip-tilt correction. The  $S/N$  could be also improved by using a photon-counting camera with a much smaller readout time. The effective integration was only 1/30 of the observing time (duty cycle 0.03), i.e. the  $S/N = 6.6$  (Table 1) corresponds to 7 s of integrated time.

Our results confirm that the stability of the gondola suspension and the associated control system are critical. More studies (theoretical and experimental) are required to better characterize high frequency vibrations, in particular if we wish to use this interferometer for astrometry, or with an adaptive optics system (adapted to a diluted telescope) for coronagraphy. Cable models have been set up (Enmark et al. 2011, Andersen et al. 2014b). A theoretical study based upon an exact numerical model of the Carlina experiment and including all cables and suspended masses is in progress and will be documented separately (Andersen et al. 2014a).

## 7. Conclusions

1. Fringes have been obtained on Deneb with 5 m baseline using a filter of 84 nm bandwidth, centred at  $\lambda = 510$  nm.
2. The results confirm that the entire system conceptually has worked correctly. They also show that, when the primary mirrors are aligned using the metrology system (Paper II), we can directly record fringes in the focal gondola, even in blind operation. The low signal to noise ratio ( $S/N = 6.6$ ) can largely be explained by oscillations of the focal gondola. Modeling suggests that if the cable preload is too low, then a gain in suspension stiffness of an order of magnitude should be possible by increasing the preload. It is also believed that a much better gondola stability could be obtained using servo-controlled reaction wheels, and reaction masses on board the gondola with appropriate angular and linear gondola acceleration, velocity and position feedback. Hence, considering these potential future improvements, we find the above results highly encouraging.
3. The Carlina-type diluted telescope concept could be interesting for an interferometer with high imaging capability and sensitivity (for example:  $> 10$  mirrors of 1–5 m each; baseline 50–100 m; near IR range; pylons to carry the optics). It could perhaps be installed at an astronomical site by digging an artificial crater. More studies are required to determine the cost of such a solution. It could be combined with auxiliary telescopes at very long baselines (for example: 0.5–1 km) by using delay lines. Such an uv coverage (dense on the shorter baselines, and more diluted on the longer ones) is similar to the ALMA radio telescope geometry, and is optimal for imaging of complex objects. This solution could be studied for the Planet Formation Imager project<sup>3</sup> proposed by Monnier et al. (2014) during the OHP2013 colloquium (Surdej & Pott 2014). Such an interferometer could also be attractive for post-ELTs 50–100 m diluted aperture. In space, the metrology from the center of curvature (Paper II) could be used to cophase the spherical primary mirrors with an extremely high accuracy.

**Acknowledgements.** This research has been funded by ASHRA, CNRS/INSU, Pytheas/OSU and Collège de France. Mechanical elements were built by the technical group at OHP and Nice observatory. Thanks to Mette Owner-Petersen for having analysed the theoretical prospects of using passive shock absorbers. Thanks to Jean Surdej, Stéphane Dumont, and Armand Rotureau for their wonderful pictures of the experiment. We are grateful to the students and to the people who helped us during the long nights of tests: Julien Chombart, Jean-Philippe Orts, Romain Pascal, Sandrine Perruchot, etc. We are very grateful to the Rouvier Lafont Manosque company that sponsored the last night (loan of the truck crane) when we obtained Fringes ! We are grateful to the LEUKOS company that helped us to use their supercontinuum laser.

## References

- Andersen, T., Le Coroller, H., Owner-Petersen, M., & Dejonghe, J. 2014a, In preparation
- Andersen, T., Le Coroller, H., Owner-Petersen, M., & Dejonghe, J. 2014b, in *Improving the Performances of Current Optical Interferometers and Future Designs*, ed. L. Arnold, H. Le Coroller, & J. Surdej, 153–173
- Berger, J.-P., Malbet, F., Baron, F., et al. 2012, *A&A Rev.*, 20, 53
- Berger, J.-P., Schanen-Duport, I., El-Sabban, S., et al. 1999, in *Astronomical Society of the Pacific Conference Series*, Vol. 194, *Working on the Fringe: Optical and IR Interferometry from Ground and Space*, ed. S. Unwin & R. Stachnik, 264
- Berio, P., Vakili, F., Mourard, D., & Bonneau, D. 1998, *A&AS*, 129, 609
- Blazit, A., Rondeau, X., Thiébaud, E., et al. 2008, *Applied Optics*, 47, 1141
- Dejonghe, J., Le Coroller, H., Deram, P., Ricci, D., & Hespeels, F. 2014, in *Improving the Performances of Current Optical Interferometers & Future Designs*, ed. L. Arnold, H. Le Coroller, & J. Surdej, 135–151
- Enmark, A., Andersen, T., Owner-Petersen, M., Chakraborty, R., & Labeyrie, A. 2011, in *Society of Photo-Optical Instrumentation Engineers (SPIE) Conference Series*, Vol. 8336, *Society of Photo-Optical Instrumentation Engineers (SPIE) Conference Series*
- Labeyrie, A. 1996, *A&AS*, 118, 517
- Lacour, S., Tuthill, P., Monnier, J. D., et al. 2014, *MNRAS*, 439, 4018
- Le Coroller, H., Dejonghe, J., Arpesella, C., Vernet, D., & Labeyrie, A. 2004, *A&A*, 426, 721, Paper I
- Le Coroller, H., Dejonghe, J., Regal, X., et al. 2012a, in *Society of Photo-Optical Instrumentation Engineers (SPIE) Conference Series*, Vol. 8445, *Society of Photo-Optical Instrumentation Engineers (SPIE) Conference Series*
- Le Coroller, H., Dejonghe, J., Regal, X., et al. 2012b, *A&A*, 539, A59, Paper II
- Mennesson, B. 2014, in *Improving the Performances of Current Optical Interferometers & Future Designs*, ed. L. Arnold, H. Le Coroller, & J. Surdej, 221–233
- Monnier, J., Krausb, S., Buscher, D., et al. 2014, *SPIE*, in press
- Perrin, G., Lai, O., Lena, P. J., & Coudé du Foresto, V. 2000, in *Society of Photo-Optical Instrumentation Engineers (SPIE) Conference Series*, Vol. 4006, *Society of Photo-Optical Instrumentation Engineers (SPIE) Conference Series*, ed. P. Léna & A. Quirrenbach, 708–714
- Rabbia, Y. 1989, in *NATO ASIC Proc. 274: Diffraction-Limited Imaging with Very Large Telescopes*, ed. D. M. Alloin & J.-M. Mariotti, 125
- Roddier, F. & Lena, P. 1984, *Journal of Optics*, 15, 363
- Surdej, J. & Pott, J.-U. 2014, in *Improving the Performances of Current Optical Interferometers and Future Designs*, ed. L. Arnold, H. Le Coroller, & J. Surdej, 277–279
- Ten Brummelaar, T. A., McAlister, H. A., Ridgway, S. T., et al. 2010, in *Society of Photo-Optical Instrumentation Engineers (SPIE) Conference Series*, Vol. 7734, *Society of Photo-Optical Instrumentation Engineers (SPIE) Conference Series*
- Woillez, J., Perrin, G., & Lai, O. 2005, in *Bulletin of the American Astronomical Society*, Vol. 37, *American Astronomical Society Meeting Abstracts*, 1308

<sup>3</sup> <http://planetformationimager.org>



## Appendix A: Logbook of the observations

The weather conditions reported in the last two columns of Table A.1 have been recorded <sup>4</sup> by the OHP meteo station located 300 m north of the experiment. Note that the anemometer is not sensitive to wind below 1 m/s. The values smaller than 1 m/s are the average wind speeds over the observation period given in the UT column. Moreover, the anemometer is located close to ground, and it is likely that the wind was somewhat stronger (due to a wind gradient) at the level of the Carlina cables. Fringes on Deneb on Sept 5. were obtained during the most quiet period of the full observing run.

**Table A.1.** Log book of September 2013 observations

Star name	mV	Images number	Date (month day)	UT (hh:mm:ss)	Exp. time (ms)	Bases (m)	Camera type	Av. seeing (arcsec.)	Av. Wind speed (m/s)
Lab. source	...	10000	July 19	...	15	5 9 10.5	science (1)	...	...
$\gamma$ And	2.10	40000	Sept. 02	02:47:00 03:24:00	10	5 9 10.5	science	1.21	0.48
$\gamma$ And	2.10	70000	Sept. 03	02:26:00 03:09:00	5	5 9 10.5	science (2)	1.2	0.25
$\gamma$ And	2.10	40000	Sept. 04	02:28:00 02:50:00	5	5 9 10.5	science	1.27	2.6
Deneb ( $\alpha$ Cyg)	1.25	3000	Sept. 05	21:08:30 21:10:00	1	5	science	0.91	0
Deneb ( $\alpha$ Cyg)	1.25	10000	Sept. 05	21:28:00 21:33:00	1	5	science	0.89	0
Sky back-ground	...	5000	Sept. 05	22:45:00 22:47:30	5	5	science	...	...
$\alpha$ And	3.62	1113	Sept. 05	22:57:00 23:00:00	100	-	guiding	...	...
$\alpha$ And	3.62	10000	Sept. 05	23:15:30 23:20:30	5	5	science	1.00	1.1
$\alpha$ And	3.62	1253	Sept. 05	23:44:00 23:48:00	100	-	guiding	...	...
$\gamma$ And	2.10	30000	Sept. 05	02:19:30 02:35:30	5	5	science	1.21	0.66
$\gamma$ And	2.10	1524	Sept. 05	02:52:00 02:57:00	100	-	guiding	...	...

**Notes.** The first line corresponds to a laboratory observation done in July 2013. The dates correspond to the beginning of the night. The UT column gives the starting and ending time of recording. *Remarks:* (1) *Laboratory Fringes*; (2) *Only NS base (9 m) at the end.*

<sup>4</sup> Seeing is measured with a SBIG seeing Monitor, see <https://www.sbig.com/products/cameras/specialty/seeing-monitor/>